ACS APPLIED MATERIALS & INTERFACES

Research Article

Cite This: ACS Appl. Mater. Interfaces 2019, 11, 3053−3060

www.acsami.org

Green Solution-Processed Tin-Based Perovskite Films for Lead-Free Planar Photovoltaic Devices

Xiao-Lei Li,[†] Li-Li Gao,[†] Qian-Qian Chu,[†] Yan Li,[‡] Bin Ding,[†] and Guan-Jun Yang*[,†]

[†]State Key Laboratory for Mechanical Behavior of Materials, School of Materials Science and Engineering, Xi'an Jiaotong University, No. 28, Xianning West Road, Xi'an 710049, China

[‡]School of Materials Science and Engineering, Xi'an Shiyou University, Xi'an 710065, China

Supporting Information

ABSTRACT: The eco-friendly Sn-based perovskites have attracted more and more attention in lead-free perovskite photovoltaic field. However, the device performance and reproducibility are greatly challenged in preparing high-quality perovskite films. Here, we fabricated uniform and dense Sn-based perovskite films via a green gas pump treatment technology. Remarkably, we successfully fabricated a large-area (>20 cm^2) Sn-based perovskite film with a mirror-like surface, which is the largest Sn-based perovskite film ever reported. Besides, we found that the phase separation phenomenon induced by excess SnF_2 was eliminated when the pressure is 1500 Pa. Finally, we fabricated highly reproducible Sn-based solar cells and obtained an inspiring efficiency of 1.85%, which is the highest reported efficiency for Sn-based devices with a configuration of fluorine-doped tin oxide/compact TiO_2/perovskite/hole transport material/electrode. Our results demonstrate the feasibility of using gas pump treatment technique to prepare high-quality Sn-based perovskite films, which paves a way for large-scale green manufacturing of Sn-based perovskite solar cells in the future.

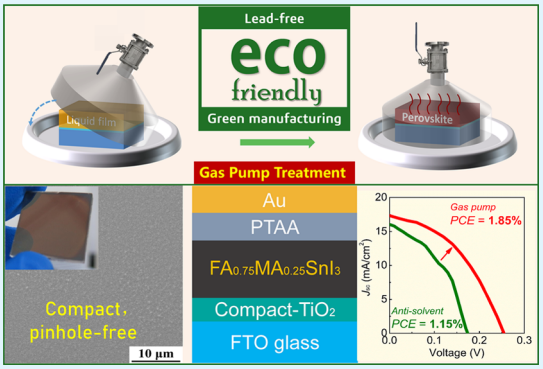

KEYWORDS: *lead-free, tin-based, gas pump treatment, green manufacturing, perovskite solar cell*

INTRODUCTION

Organic−inorganic hybrid lead halide perovskite solar cells (PVSCs) have emerged as the most promising candidates for high-efficiency low-cost photovoltaic (PV) technology.[1−5] To date, the solar-to-electric power conversion efficiency (PCE) of PVSCs has been verified at an ultrahigh 23.3%.[6] Recently, Cao et al.[7] and Lin et al.[8] independently reported perovskite light-emitting diodes with external quantum efficiency exceeding 20%. However, all top-performing optoelectronic devices[9−13] were based on toxic Pb-containing perovskite materials, which might influence the ultimate fate of this technology.[14,15] The utilization of Pb-containing materials in electronic devices is strictly restricted by the European Union and other countries.[16] In addition, Pb-based perovskite materials exhibit band gap (E_g) between 1.48 and 2.3 eV, which is higher than the ideal E_g (1.34 eV).[17] Consequently, it has been regarded as forceful incentive stimulating more research effort to develop Pb-free PVSCs.

To overcome the toxicity issue, several eco-friendly metal elements were used to replace Pb in perovskite materials,[18−23] such as Sn,[24−28] Bi,[29,30] and Cu.[31−33] Among these, Sn-based perovskites appear to be the most efficient PV materials for Pb-free PVSCs. First, Sn-based perovskites possess three-dimensional structural and electronic dimensionalities as that found in the Pb-based perovskites.[34] Second, Sn-based perovskites exhibit promising carrier diffusion length (>500 nm),[35] extremely high charge-carrier mobility, high absorption coefficients, and low exciton binding energies.[24,36] Third, Sn-based perovskites exhibit slightly narrower E_g (1.3−1.4 eV) than their lead analogues,[24,36] which is a near-ideal value for single-junction solar cells according to the Shockley−Queisser efficiency limit (33%).[37]

In 2014, Hao et al.[38] and Noel et al.[39] independently reported $MASnI_3$ (MA = CH_3NH_3) as a light absorber in a typical n−i−p device consisting of a mesoporous TiO_2 (meso-TiO_2) scaffold with efficiencies of around 6% via conventional one-step spin-coating method. However, the reproducibility of the results needs to be enhanced.[36] For normal architecture, high-efficiency solar cells were usually obtained in a configuration of fluorine-doped tin oxide (FTO)/compact TiO_2 (c-TiO_2)/meso-TiO_2/perovskite/hole transport material (HTM)/electrode.[24,36] Several groups achieved significant breakthroughs for Sn-based PVSCs with mesoporous n−i−p architecture. For instance, Kanatzidis et al. developed a series of strategies to improve the morphology and device performance, including ethylenediammonium cations,[40,41] diammonium cations,[42] piperazine,[43] and reducing atmosphere process.[44,45] One of the reasons for meso-TiO_2 layer necessary

Received: November 1, 2018
Accepted: December 26, 2018
Published: December 26, 2018

DOI: 10.1021/acsami.8b19143
ACS Appl. Mater. Interfaces 2019, 11, 3053−3060

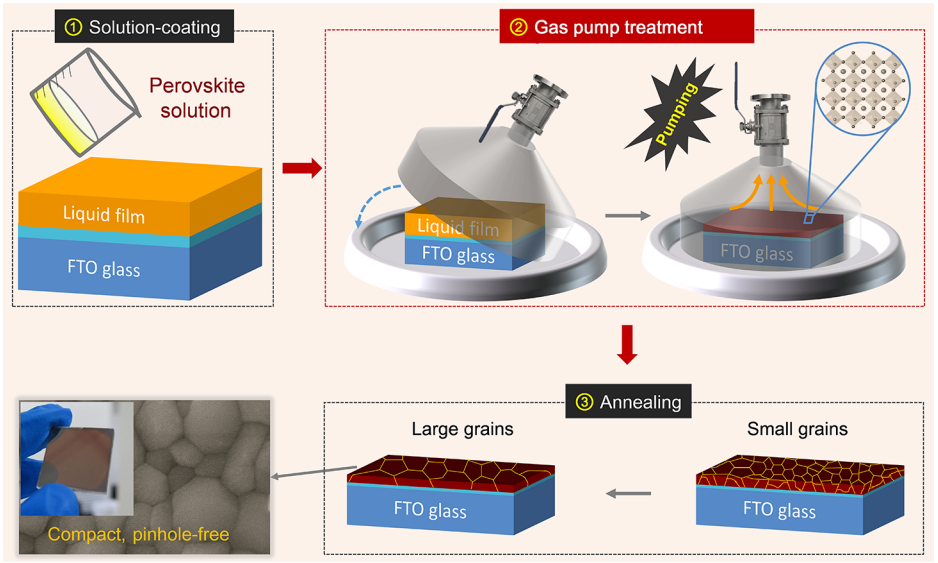

Figure 1. Gas pump treatment procedure for preparing a uniform and dense perovskite film.

might be associated with the difficulty of preparing uniform and dense films on c-TiO_2 substrates via conventional one-step spin-coating method.[40−42] However, the use of meso-TiO_2 layer adds one more step to the fabrication process, which is perhaps disadvantageous for scalable fabrication and application.[46]

In 2016, Qi et al. reported a normal planar device with the configuration of FTO/c-TiO_2/$CH_3NH_3SnBr_3$/P3HT/Au and achieved a PCE of ∼1% by sequential vapor deposition.[47] Kanatzidis et al. reported a normal planar device with the configuration of FTO/c-TiO_2 layer/$CH_3NH_3SnI_3$/poly[bis(4-phenyl)(2,4,6-trimethylphenyl)amine] (PTAA)/Au and achieved a low PCE of ∼0.3%.[35] Later, Wang et al. reported a Sn-based planar device (FTO/c-TiO_2/$CsSnI_3$/spiro-OMeTAD/Au) and achieved a PCE of 0.77%.[48] Despite substantial effort, to date, the efficiency of planar n−i−p architecture (FTO/c-TiO_2/perovskite/HTM/electrode) is still seriously lags far behind state-of-the-art mesoporous n−i−p architecture (FTO/c-TiO_2/m-TiO_2/perovskite/HTM/electrode, PCE = 7.23%),[49] implying that more effective techniques are urgently needed to promote the thin film quality as well as the device performance.

In this article, for the first time, we successfully fabricated a uniform and dense Sn-based perovskite film on c-TiO_2 substrate by gas pump treatment technology. Compared with the highly toxic antisolvent treatment, our gas pump treatment technology is an environmental friendly tool for the fabrication of high-quality perovskite films. Furthermore, we demonstrate that this method can be used to fabricate large-area (>20 cm^2) Sn-based perovskite films. Eventually, we were able to fabricate highly reproducible $FA_{0.75}MA_{0.25}SnI_3$-based PVSCs and obtained an inspiring efficiency of 1.85%, which is the highest reported efficiency for Sn-based devices with the configuration of FTO/c-TiO_2/perovskite/HTM/electrode.

■ RESULTS AND DISCUSSION

Herein, we choose mixed cation perovskites $FA_{0.75}MA_{0.25}SnI_3$ (FA = $CH(NH_2)_2$) with a near-ideal E_g of 1.33 eV as light absorber layers.[27,50,51] The gas pump process includes three stages, as depicted in Figure 1. First stage, Sn-based perovskite precursor solution is coated over the entire surface of the c-TiO_2/FTO substrate to form a perovskite wet-solution film. The wet-solution film can be deposited by spin-coating and other scalable solution deposition methods (for example, blade coating, slot-die coating, spray coating, and inkjet printing).[52] Second stage, the resulting sample is then placed for a few seconds into a home-made low-pressure chamber to boost uniform nuclei of the Sn-based perovskite by removing most of the solvents rapidly. The solvents in perovskite wet-solution film at low environmental pressure have lower boiling points than when solvents are at atmospheric pressure. Therefore, the evaporation of solvents occurs rapidly when the resulting sample is placed into a low-pressure chamber. Within 10 s after starting pumping the gas, a dark red somewhat transparent film with a mirror-like surface is obtained. Third stage, after heating on the hotplate, a highly uniform and pinhole-free $FA_{0.75}MA_{0.25}SnI_3$ film with big grains can be achieved.

To clarify the influence of the chamber pressure on the perovskite film quality, $FA_{0.75}MA_{0.25}SnI_3$ films were fabricated by the gas pump treatment at different pressures from 20 to 4000 Pa. We obtained uniform, dense, and full-coverage Sn-based perovskite films when the pressure is from 20 to 1500 Pa (see Figure S2b,c,e,f,h,i), which is a wide process window. Obviously, there are some white spots existed in the Sn-based perovskite films (see Figure S2b,c,e,f,k,l,n,o). The white spots might be associated with the phase separation induced by SnF_2.[50,53] Surprisingly, the white spots were almost eliminated when the pressure reached 1500 Pa (see Figure S2h,i). This implies that suitable pressure contributes to the elimination of the phase separation induced by excess SnF_2. This phenomenon is consistent with the homogeneous dispersion of SnF_2 via chemical method (SnF_2−pyrazine complex).[53] Many pinholes/voids existed in the perovskite films and bared the substrates when pressure reached 3000 and 4000 Pa (Figure S2k,l,n,o). The reason for this phenomenon is that high pressure over 3000 Pa cannot significantly accelerate the evaporation of the solvents in perovskite wet-solution film.[54]

Figure 2 shows the photographs, scanning electron microscopy (SEM) images, and illustrations of nucleation growth processes of the $FA_{0.75}MA_{0.25}SnI_3$ perovskite films fabricated by heat drying treatment, antisolvent treatment, and gas pump treatment. As shown in Figure 2a,b, the

DOI: 10.1021/acsami.8b19143
ACS Appl. Mater. Interfaces 2019, 11, 3053−3060

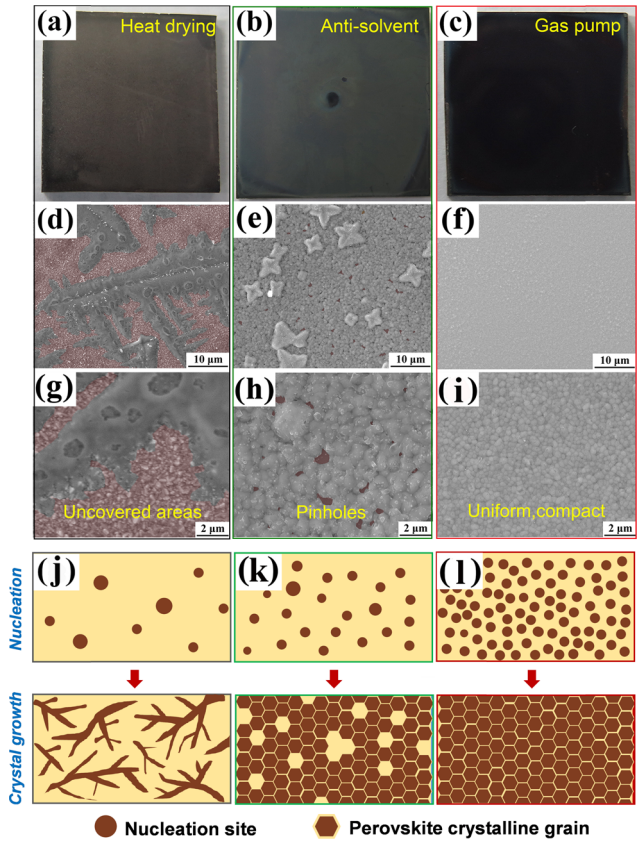

Figure 2. Photographs, low- and high-magnification SEM images, and illustrations of nucleation growth processes of samples prepared by three methods: (a, d, g, j) heat drying method, (b, e, h, k) antisolvent treatment, and (c, f, i, l) gas pump treatment.

$FA_{0.75}MA_{0.25}SnI_3$ perovskite films fabricated by the heat drying method and antisolvent treatment were hazy and rough. In contrast, the $FA_{0.75}MA_{0.25}SnI_3$ film prepared by the gas pump treatment was black and smooth (Figure 2c). Furthermore, obvious differences among the $FA_{0.75}MA_{0.25}SnI_3$ perovskite films prepared by three methods can be observed from SEM images. For the heat drying treatment, the film shows dendritic morphology with very poor coverage (see Figure 2d,g). The result is associated with the serious localized solute accumulation because of the slow solvent evaporation of the heat drying treatment (Figure 2j).[55] For antisolvent treatment, the film exhibits rough morphology with numerous pinholes (see Figure 2e,h,k), which is similar with previously reported results.[27,56] In contrast, the gas pump treatment yielded uniform and dense Sn-based perovskite films without pinholes (see Figure 2f,i,l, and Figure S1). Perovskite growth in solution is a process that combines supersaturation, nucleation, and crystal growth. A high density of nucleation sites and a short crystal growth time are key factors for the formation of uniform and dense perovskite films.[57] Rapid solvent evaporation from precursor solutions during gas pump treatment increases the supersaturation, leading to a higher density of nucleation sites and a shorter crystal growth time, and then induces fast crystallization of uniformly sized Sn-based perovskite grains. On the basis of abovementioned satisfactory results, we anticipated that this green solution-processed technology can be used to prepare other high-quality Pb-free perovskite films in the future.

Another important obstacle that Sn-based perovskite PV technology faced is the lack of large-area films fabrication techniques. Thus, we try to fabricate a large-area Sn-based perovskite film with a size of 20.25 cm^2 by our gas pump treatment at a pressure of 1500 Pa. As shown in Figure 3a, the

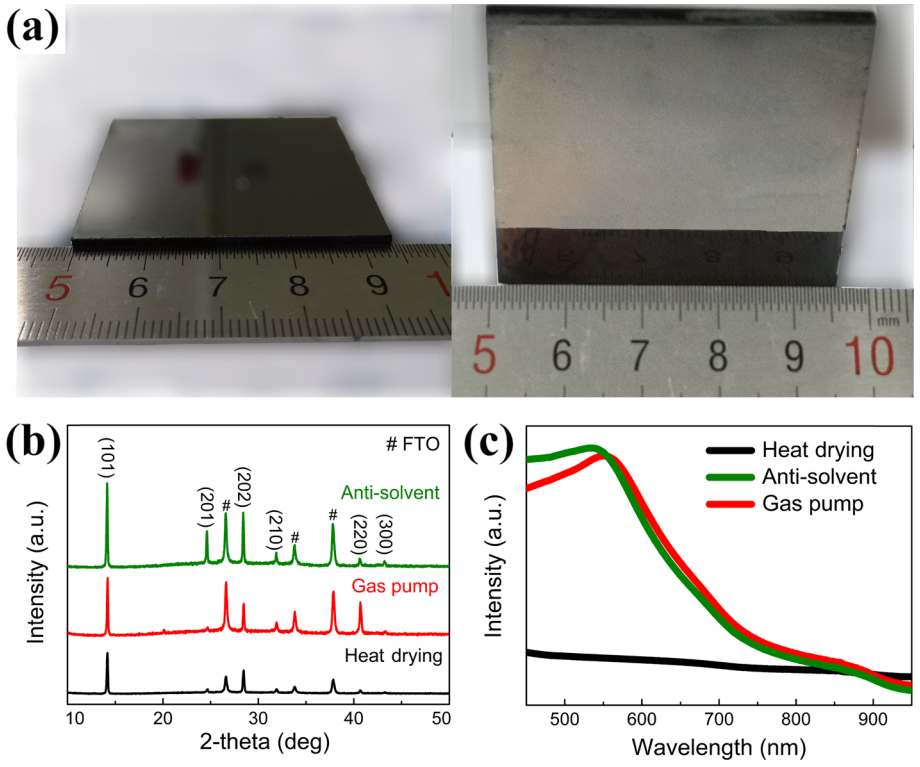

Figure 3. (a) Photographs of the large-area (20.25 cm^2) Sn-based perovskite film fabricated by the gas pump treatment. (b) XRD patterns and (c) UV−vis spectra of samples prepared by heat drying method, antisolvent treatment, and gas pump treatment.

DOI: 10.1021/acsami.8b19143
ACS Appl. Mater. Interfaces 2019, 11, 3053−3060

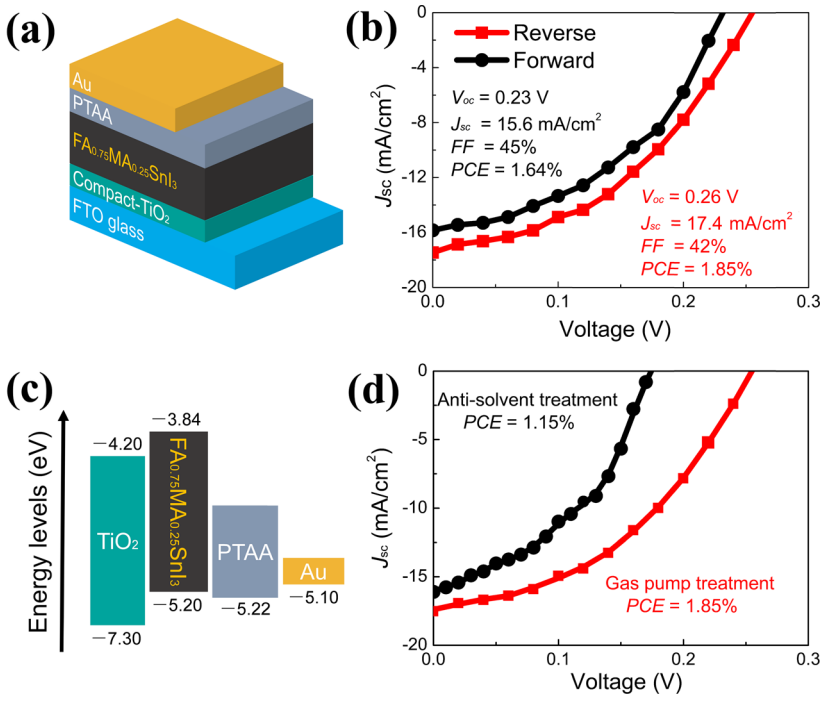

Figure 4. (a) Schematic illustration of the device configuration. (b) $J-V$ curves recorded in reverse (from V_{oc} to J_{sc}) and forward (from J_{sc} to V_{oc}) scanning direction. (c) Schematic energy band diagram of $FA_{0.75}MA_{0.25}SnI_3$-based solar cell. The energy levels of TiO_2, $FA_{0.75}MA_{0.25}SnI_3$, and PTAA were extracted from literature.[51,59] (d) $J-V$ curves of the champion Sn-based devices prepared by the antisolvent treatment and gas pump treatment.

large-area Sn-based perovskite film fabricated by the gas pump treatment exhibits a mirror-like surface. To the best of our knowledge, this is the first time to report a high-quality and large-area Sn-based perovskite film exceeding 20 cm^2. For comparison, we fabricated large-area Sn-based perovskite films by the heat drying treatment and antisolvent treatment. The films prepared by the heat drying treatment and antisolvent treatment were rough and gray (Figure S3). The above-mentioned results indicate that gas pump treatment is an effective method for creating a high-quality Sn-based perovskite film, which is beneficial for the scalable fabrication of Sn-based perovskite thin-film PV technology in the future.

To investigate the effect of the three methods on the crystallinity of $FA_{0.75}MA_{0.25}SnI_3$ perovskite films, we carried out X-ray diffraction (XRD) measurements of these samples. As shown in Figure 3b, all samples exhibit a single phase of $FA_{0.75}MA_{0.25}SnI_3$, which have well-matched XRD patterns with previously reported orthorhombic crystal structure of $FA_{0.75}MA_{0.25}SnI_3$ perovskite.[27,50,51] Besides, all samples show similar XRD patterns of $FA_{0.75}MA_{0.25}SnI_3$, indicating that the effect of different methods on the formation of the crystalline phase is not considerable. The UV−vis spectra of the $FA_{0.75}MA_{0.25}SnI_3$ perovskite films prepared by three methods are shown in Figure 3c. The gas pump- and antisolvent-processed films exhibit much stronger absorbance in the range from 450 to 900 nm than that of the heat drying treatment. The low absorption intensity of the sample prepared by the heat drying treatment mainly could be associated with the incomplete coverage region (see Figure 2d,g).[58] The UV−vis absorption intensity of the gas pump-processed $FA_{0.75}MA_{0.25}SnI_3$ perovskite film is slightly stronger than that of the antisolvent-processed sample.

Using gas pump-processed Sn-based perovskite films, we fabricated solar cells with an architecture of FTO/c-TiO_2/$FA_{0.75}MA_{0.25}SnI_3$/PTAA/Au (Figure 5a and Figure S4). N-type TiO_2 was used as an electron transport material (ETM), which was verified as an outstanding ETM in Pb-based PVSCs, and p-type PTAA was used as an HTM.[41,42] Figure 5b shows the current density−voltage ($J-V$) characteristic of a champion solar cell prepared by the gas pump treatment, measured under reverse and forward voltage scanning. The device achieved a PCE of 1.85% with a photocurrent density (J_{sc}) of 17.4 mA/cm^2, an open-circuit voltage (V_{oc}) of 0.26 V, and a fill factor (FF) of 42% when measured under reverse voltage scanning and a PCE of 1.64% with a V_{oc} of 0.23 V, a J_{sc} of 15.6 mA/cm^2, and an FF of 45% when measured under forward voltage scanning. The hysteresis phenomenon shown in Figure 5b is consistent with previously reported results.[59] Furthermore, the integrated J_{sc} calculated from the incident photon-to-current efficiency (IPCE) spectrum is about 16.3 mA/cm^2, which is very close to the J_{sc} obtained from the $J-V$ curves (Figure S5). Despite the performance (PCE, 1.85%) was not fully optimized, it is the highest reported efficiency so far for Sn-based devices with a configuration of FTO/c-TiO_2/perovskite/HTM/electrode. To compare with other planar structure device without a meso-TiO_2 layer, the detailed PV parameters are summarized in Table S1. The voltage deficit of gas pump-processed Sn-based devices is comparable with previously reported results (see Table S1). To date, the low V_{oc} in such system has not been well understood. On the one hand, the maximum V_{oc} is typically decided by the built-in potential barrier (V_{bi}) of Sn-based perovskite solar cells, namely, the difference of the highest occupied molecular orbital of PTAA and the conduction band of Sn-based perovskite.[60] Therefore, more efforts should focus on optimizing the band alignment of the devices (see Figure 4c) to further improve the V_{oc}. On the other hand, the poor V_{oc} in such system can be traced back to the high p-type defect

DOI: 10.1021/acsami.8b19143
ACS Appl. Mater. Interfaces 2019, 11, 3053−3060

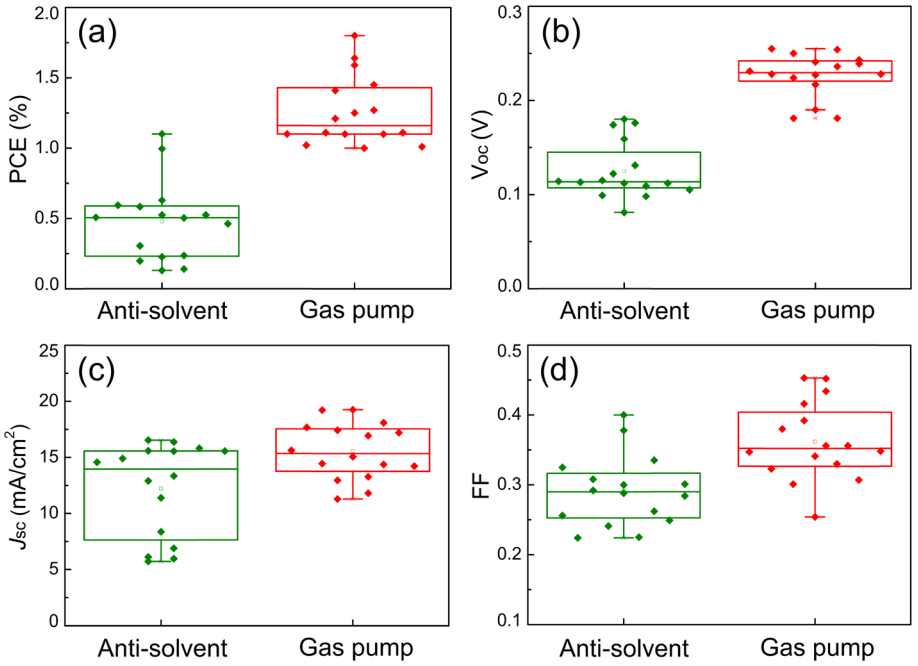

Figure 5. PV metrics for 16 devices fabricated by the antisolvent treatment and gas pump treatment. (a) PCE, (b) V_{oc}, (c) J_{sc}, and (d) FF.

states[24] (electron and hole trap centers) caused by the easy oxidization of Sn^{2+} during device fabrication. To move forward, more efforts should be devoted to the suppression of the oxidization of Sn^{2+} to reduce defect states, for example, incorporating new antioxidants (sodium hydrogen sulfite or ethoxyquin) into the precursor solution to reduce the oxidization of Sn^{2+}. As shown in Figure 4d, the gas pump-processed device achieved a champion PCE of 1.85%, which is higher than that of the antisolvent-treated device (PCE, 1.15%).

To further compare the reproducibility of the devices, we fabricated 16 devices by the gas pump treatment and antisolvent treatment. As shown in Figure 5, gas pump treatment greatly improved device performance and reproducibility compared to the antisolvent treatment. The performance of the devices prepared by the antisolvent treatment is relatively low, with an average PCE of 0.48 ± 0.28%, compared with an average PCE of 1.27 ± 0.25% of the devices prepared by the gas pump treatment (see Figure 5a, Tables S2 and S3). The V_{oc} of the devices with anti-solvent and gas pump treatment increases from 0.125 ± 0.030 V of the anti-solvent treated devices to 0.226 ± 0.024 V of the gas pump- processed devices, and the FF increases from 29.3 ± 5.3 to 36.2 ± 5.6%, leading to the remarkable enhancement in PCE. The improvement of device parameters and reproducibility can be attributed to the higher uniformity and pinhole-less characteristic of the gas pump-processed $FA_{0.75}MA_{0.25}SnI_3$ films, which can eliminate the direct contact of HTM and ETM (Figure 2c,f,i). The abovementioned results reveal the high reproducibility of Sn-based PVSCs prepared by the gas pump treatment technique.

CONCLUSIONS

In conclusion, we successfully fabricated high-quality Sn-based perovskite films by an eco-friendly gas pump treatment technology. We found that the phase separation phenomenon induced by excess SnF_2 was eliminated when the pressure is 1500 Pa. Furthermore, we demonstrate that this method can be used to fabricate a large-area (>20 cm^2) Sn-based perovskite film with a mirror-like surface, which is an effective way for the large-scale fabrication of Sn-based PVSCs. Finally, we fabricated highly reproducible $FA_{0.75}MA_{0.25}SnI_3$-based solar cells and obtained an inspiring efficiency of 1.85%, which is the highest reported efficiency for Sn-based devices with a configuration of FTO/c-TiO_2/perovskite/HTM/electrode. Taken together, this work will open a new door for green manufacturing of high-quality lead-free perovskite films in the future.

EXPERIMENTAL SECTION

Materials. All the chemicals and reagents were used as received without further purification, including SnI_2 (99.99%, Sigma-Aldrich), SnF_2 (>99%, Sigma-Aldrich), and tetrakis(pentafluorophenyl)borate (TPFB) (Tokyo Chemical Industry Co., Ltd.). Formamidinium iodide ($NH_2CH{=}NH_2I$, FAI), methylammonium iodide (CH_3NH_3I, MAI), and PTAA were purchased from Xi'an Polymer Light Technology Corp. (China). *N*,*N*-dimethylformamide (DMF, anhydrous, 99.8%), dimethyl sulfoxide (DMSO, anhydrous, 99.9%), chlorobenzene (anhydrous, 99.5%), and FTO-coated glass (TEC7, 2.2 mm) patterned using a laser were purchased from Ying Kou You Xuan Trade Co., Ltd. (China). All solutions were filtered through a 0.22 μm filter before use.

Thin Film Fabrication. Stoichiometric FAI (387 mg), MAI (119.3 mg), SnI_2 (1116 mg), and SnF_2 (48 mg) were dissolved in a mixture of 4.286 mL of DMF and 0.714 mL of DMSO. Then, the $FA_{0.75}MA_{0.25}SnI_3$ precursor solution was stirred at 70 °C for 1 h. For the heat drying treatment, the precursor solution was dropped on the c-TiO_2 layer and spin-coated at 4000 rpm for 30 s. For the antisolvent treatment, the precursor solution was dropped on the c-TiO_2 layer and spin-coated at 4000 rpm for 30 s. Chlorobenzene (200 μL) was dripped onto the spinning substrate during the spin-coating. For the gas pump treatment, the precursor solution was dropped on the c-TiO_2 layer and spin-coated at 4000 rpm for 10 s. Subsequently, the sample was immediately transferred to a home-developed gas pump chamber with 1500 Pa, pumping the sample for 10 s. All perovskite films were made and annealed at 70 °C for 15 min in a glovebox.

DOI: 10.1021/acsami.8b19143
ACS Appl. Mater. Interfaces 2019, 11, 3053−3060

Device Fabrication. FTO substrates were cleaned by sonicating sequentially in acetone, ethanol, and deionized water, each for 15 min, then dried by nitrogen, and treated in UV ozone for 30 min. A c-TiO_2 layer was prepared according to our previously report.[13] The c-TiO_2/FTO substrate was transferred into a glovebox for the preparation of a perovskite layer (O_2 < 0.1 ppm, H_2O < 0.1 ppm). Then, $FA_{0.75}MA_{0.25}SnI_3$ precursor solution was dropped on the c-TiO_2 layer and spin-coated at 4000 rpm for 10 s. Subsequently, the sample was immediately transferred to a home-made gas pump chamber[3] with 1500 Pa, pumping the sample for 10 s. Then, a somewhat mirror-like dried Sn-based perovskite film was heated at 70 °C for 15 min. The solution of hole transporting material, consisting of 32 mg of PTAA and 3.6 mg of TPFB in 1.6 mL of chlorobenzene, was spin-coated on the Sn-based perovskite film at 1500 rpm for 30 s and then annealed at 70 °C for 5 min. Finally, Au metal electrode was thermally evaporated. Devices were encapsulated with cover glass and UV hard resin (Ausbond, A350).

Film and Device Characterization. XRD measurements were carried out on an Ultima IV X-ray diffractometer with Cu Kα from 10 to 80° (2θ). UV−vis spectra were measured with the $FA_{0.75}MA_{0.25}SnI_3$ films spin-coated on FTO substrates using a PerkinElmer Lambda 950 spectrophotometer. SEM tests were performed on a field-emission SEM (MIRA3 TESCAN). The exact light intensity of the solar simulator was calibrated by a standard Si reference cell (91150V, Oriel). J−V curves of the solar cells with an active area of 0.1 cm^2 were tested by using a source meter (Keithley, 2400) under 100 mW/cm^2 illumination using a solar simulator (Peccell Technologies, PEC-L01). The devices were measured by reverse (from 1.2 to −0.2 V) and forward (from −0.2 to 1.2 V) voltage scanning with a scan rate of 0.01 V/s. J−V curves that were finished in a N_2-filled glovebox. IPCE spectrum was collected by a solar cell quantum efficiency measurement system (SolarCellScan 100, Zolix Instruments Co., Ltd.). The IPCE test was performed under ambient conditions.

■ ASSOCIATED CONTENT

Supporting Information

The Supporting Information is available free of charge on the ACS Publications website at DOI: 10.1021/acsami.8b19143.

Experimental details, SEM images and photographs of $FA_{0.75}MA_{0.25}SnI_3$ samples, tables, SEM image of a complete device, and IPCE (PDF)

■ AUTHOR INFORMATION

Corresponding Author

*E-mail: ygj@mail.xjtu.edu.cn.

ORCID

Xiao-Lei Li: 0000-0003-4913-0028

Yan Li: 0000-0001-6017-3104

Guan-Jun Yang: 0000-0002-7753-3636

Notes

The authors declare no competing financial interest.

■ ACKNOWLEDGMENTS

This work was financially supported by the National Program for Support of Top-notch Young Professionals. We also thank the Instrument Analysis Center of Xi'an Jiaotong University for performing various characterization and measurements.

■ REFERENCES

(1) Brenner, T. M.; Egger, D. A.; Kronik, L.; Hodes, G.; Cahen, D. Hybrid Organic−Inorganic Perovskites: Low-Cost Semiconductors with Intriguing Charge-Transport Properties. *Nat. Rev. Mater.* **2016**, *1*, 15007.

(2) Zhou, G.; Wu, J.; Zhao, Y.; Li, Y.; Shi, J.; Li, Y.; Wu, H.; Li, D.; Luo, Y.; Meng, Q. Application of Cesium on the Restriction of Precursor Crystallization for Highly Reproducible Perovskite Solar Cells Exceeding 20% Efficiency. *ACS Appl. Mater. Interfaces* **2018**, *10*, 9503−9513.

(3) Ding, B.; Gao, L.; Liang, L.; Chu, Q.; Song, X.; Li, Y.; Yang, G.; Fan, B.; Wang, M.; Li, C.; Li, C. Facile and Scalable Fabrication of Highly Efficient Lead Iodide Perovskite Thin-Film Solar Cells in Air Using Gas Pump Method. *ACS Appl. Mater. Interfaces* **2016**, *8*, 20067−20073.

(4) Wu, Y.; Yang, X.; Chen, W.; Yue, Y.; Cai, M.; Xie, F.; Bi, E.; Islam, A.; Han, L. Perovskite Solar Cells with 18.21% Efficiency and Area over 1 cm^2 Fabricated by Heterojunction Engineering. *Nat. Energy* **2016**, *1*, 16148.

(5) Rong, Y.; Hu, Y.; Mei, A.; Tan, H.; Saidaminov, M. I.; Seok, S. I.; McGehee, M. D.; Sargent, E. H.; Han, H. Challenges for Commercializing Perovskite Solar Cells. *Science* **2018**, *361*, eaat8235.

(6) NREL Chart. https://www.nrel.gov/pv/assets/images/efficiency-chart.png (accessed October 10, 2018).

(7) Cao, Y.; Wang, N.; Tian, H.; Guo, J.; Wei, Y.; Chen, H.; Miao, Y.; Zou, W.; Pan, K.; He, Y.; et al. Perovskite Light-Emitting Diodes Based on Spontaneously Formed Submicrometre-Scale Structures. *Nature* **2018**, *562*, 249−253.

(8) Lin, K.; Xing, J.; Quan, L. N.; de Arquer, F. P. G.; Gong, X.; Lu, J.; Xie, L.; Zhao, W.; Zhang, D.; Yan, C.; et al. Perovskite Light-Emitting Diodes with External Quantum Efficiency exceeding 20 Per Cent. *Nature* **2018**, *562*, 245−248.

(9) Zhou, H.; Fan, L.; He, G.; Yuan, C.; Wang, Y.; Shi, S.; Sui, N.; Chen, B.; Zhang, Y.; Yao, Q.; et al. Low Defects, Large Area and High Stability of All-Inorganic Lead Halide Perovskite $CsPbBr_3$ Thin Films with Micron-Grains via Heat-Spraying Process for Self-Driven Photodetector. *RSC Adv.* **2018**, *8*, 29089−29095.

(10) Liu, Z.; Zhong, Y.; Sun, B.; Liu, X.; Han, J.; Shi, T.; Tang, Z.; Liao, G. Novel Integration of Perovskite Solar Cell and Supercapacitor Based on Carbon Electrode for Hybridizing Energy Conversion and Storage. *ACS Appl. Mater. Interfaces* **2017**, *9*, 22361−22368.

(11) Zou, S.; Liu, Y.; Li, J.; Liu, C.; Feng, R.; Jiang, F.; Li, Y.; Song, J.; Zeng, H.; Hong, M.; Chen, X. Stabilizing Cesium Lead Halide Perovskite Lattice through Mn(II) Substitution for Air-Stable Light-Emitting Diodes. *J. Am. Chem. Soc.* **2017**, *139*, 11443−11450.

(12) Luo, D.; Yang, W.; Wang, Z.; Sadhanala, A.; Hu, Q.; Su, R.; Shivanna, R.; Trindade, G. F.; Watts, J. F.; Xu, Z.; et al. Enhanced Photovoltage for Inverted Planar Heterojunction Perovskite Solar Cells. *Science* **2018**, *360*, 1442−1446.

(13) Ding, B.; Huang, S.-Y.; Chu, Q.-Q.; Li, Y.; Li, C.-X.; Li, C.-J.; Yang, G.-J. Low-Temperature SnO_2-Modified TiO_2 Yields Record Efficiency for Normal Planar Perovskite Solar Modules. *J. Mater. Chem. A* **2018**, *6*, 10233−10242.

(14) Babayigit, A.; Ethirajan, A.; Muller, M.; Conings, B. Toxicity of Organometal Halide Perovskite Solar Cells. *Nat. Mater.* **2016**, *15*, 247−251.

(15) Kamat, P. V.; Bisquert, J.; Buriak, J. Lead-Free Perovskite Solar Cells. *ACS Energy Lett.* **2017**, *2*, 904−905.

(16) Lotsch, B. V. New Light on an Old Story: Perovskites Go Solar. *Angew. Chem., Int. Ed.* **2014**, *53*, 635−637.

(17) Stoumpos, C. C.; Malliakas, C. D.; Kanatzidis, M. G. Semiconducting Tin and Lead Iodide Perovskites with Organic Cations: Phase Transitions, High Mobilities, and Near-Infrared Photoluminescent Properties. *Inorg. Chem.* **2013**, *52*, 9019−9038.

(18) Ju, M.-G.; Chen, M.; Zhou, Y.; Dai, J.; Ma, L.; Padture, N. P.; Zeng, X. C. Toward Eco-friendly and Stable Perovskite Materials for Photovoltaics. *Joule* **2018**, *2*, 1231−1241.

(19) Liang, L.; Gao, P. Lead-Free Hybrid Perovskite Absorbers for Viable Application: Can We Eat the Cake and Have It Too? *Adv. Sci.* **2018**, *5*, 1700331.

(20) Zhou, H.; Liu, X.; He, G.; Fan, L.; Shi, S.; Wei, J.; Xu, W.; Yuan, C.; Chai, N.; Chen, B.; et al. Synthesis, Crystal Structure, UV−Vis Adsorption Properties, Photoelectric Behavior, and DFT Computational Study of All-Inorganic and Lead-Free Copper Halide Salt $K_2Cu_2Cl_6$. *ACS Omega* **2018**, *3*, 14021−14026.

DOI: 10.1021/acsami.8b19143
ACS Appl. Mater. Interfaces 2019, 11, 3053−3060

(21) Yin, J.; Shi, S.; Wei, J.; He, G.; Fan, L.; Guo, J.; Zhang, K.; Xu, W.; Yuan, C.; Wang, Y.; et al. Earth-Abundant and Environment Friendly Organic−Inorganic Hybrid Tetrachloroferrate Salt $CH_3NH_3FeCl_4$: Structure, Adsorption Properties and Photoelectric Behavior. *RSC Adv.* **2018**, *8*, 19958−19963.
(22) Zhou, H.; Cui, X.; Yuan, C.; Cui, J.; Shi, S.; He, G.; Wang, Y.; Wei, J.; Pu, X.; Li, W.; et al. Band-Gap Tuning of Organic−Inorganic Hybrid Palladium Perovskite Materials for a Near-Infrared Optoelectronics Response. *ACS Omega* **2018**, *3*, 13960−13966.
(23) Nie, Z.; Yin, J.; Zhou, H.; Chai, N.; Chen, B.; Zhang, Y.; Qu, K.; Shen, G.; Ma, H.; Li, Y.; et al. Layered and Pb-Free Organic-Inorganic Perovskite Materials for Ultraviolet Photoresponse: (010)-Oriented $(CH_3NH_3)_2MnCl_4$ Thin Film. *ACS Appl. Mater. Interfaces* **2016**, *8*, 28187−28193.
(24) Ke, W.; Stoumpos, C. C.; Kanatzidis, M. G. "Unleaded" Perovskites: Status Quo and Future Prospects of Tin-Based Perovskite Solar Cells. *Adv. Mater.* **2018**, 1803230.
(25) Umari, P.; Mosconi, E.; De Angelis, F. Relativistic GW Calculations on $CH_3NH_3PbI_3$ and $CH_3NH_3SnI_3$ Perovskites for Solar Cell Applications. *Sci. Rep.* **2014**, *4*, 4467.
(26) Chen, K.; Wu, P.; Yang, W.; Su, R.; Luo, D.; Yang, X.; Tu, Y.; Zhu, R.; Gong, Q. Low-Dimensional Perovskite Interlayer for Highly Efficient Lead-Free Formamidinium Tin Iodide Perovskite Solar Cells. *Nano Energy* **2018**, *49*, 411−418.
(27) Liu, X.; Yan, K.; Tan, D.; Liang, X.; Zhang, H.; Huang, W. Solvent Engineering Improves Efficiency of Lead-free Tin-based Hybrid Perovskite Solar Cells beyond 9%. *ACS Energy Lett.* **2018**, *3*, 2701−2707.
(28) Wang, F.; Jiang, X.; Chen, H.; Shang, Y.; Liu, H.; Wei, J.; Zhou, W.; He, H.; Liu, W.; Ning, Z. 2D-Quasi-2D-3D Hierarchy Structure for Tin Perovskite Solar Cells with Enhanced Efficiency and Stability. *Joule* **2018**, *2*, 2732.
(29) Singh, T.; Kulkarni, A.; Ikegami, M.; Miyasaka, T. Effect of Electron Transporting Layer on Bismuth-Based Lead-Free Perovskite $(CH_3NH_3)_3Bi_2I_9$ for Photovoltaic Applications. *ACS Appl. Mater. Interfaces* **2016**, *8*, 14542−14547.
(30) Jain, S. M.; Phuyal, D.; Davies, M. L.; Li, M.; Philippe, B.; De Castro, C.; Qiu, Z.; Kim, J.; Watson, T.; Tsoi, W. C.; et al. An Effective Approach of Vapour Assisted Morphological Tailoring for Reducing Metal Defect Sites in Lead-Free, $(CH_3NH_3)_3Bi_2I_9$ Bismuth-Based Perovskite Solar Cells for Improved Performance and Long-Term Stability. *Nano Energy* **2018**, *49*, 614−624.
(31) Cortecchia, D.; Dewi, H. A.; Yin, J.; Bruno, A.; Chen, S.; Baikie, T.; Boix, P. P.; Grätzel, M.; Mhaisalkar, S.; Soci, C.; Mathews, N. Lead-Free $MA_2CuCl_xBr_{4-x}$ Hybrid Perovskites. *Inorg. Chem.* **2016**, *55*, 1044−1052.
(32) Li, X.; Li, B.; Chang, J.; Ding, B.; Zheng, S.; Wu, Y.; Yang, J.; Yang, G.; Zhong, X.; Wang, J. $(C_6H_5CH_2NH_3)_2CuBr_4$: A Lead-Free, Highly Stable Two-Dimensional Perovskite for Solar Cell Applications. *ACS Appl. Energy Mater.* **2018**, *1*, 2709−2716.
(33) Li, X.; Zhong, X.; Hu, Y.; Li, B.; Sheng, Y.; Zhang, Y.; Weng, C.; Feng, M.; Han, H.; Wang, J. Organic−Inorganic Copper(II)-Based Material: A Low-Toxic, Highly Stable Light Absorber for Photovoltaic Application. *J. Phys. Chem. Lett.* **2017**, *8*, 1804−1809.
(34) Xiao, Z.; Meng, W.; Wang, J.; Mitzi, D. B.; Yan, Y. Searching for Promising New Perovskite-Based Photovoltaic Absorbers: The Importance of Electronic Dimensionality. *Mater. Horiz.* **2017**, *4*, 206−216.
(35) Ma, L.; Hao, F.; Stoumpos, C. C.; Phelan, B. T.; Wasielewski, M. R.; Kanatzidis, M. G. Carrier Diffusion Lengths of over 500 nm in Lead-Free Perovskite $CH_3NH_3SnI_3$ Films. *J. Am. Chem. Soc.* **2016**, *138*, 14750−14755.
(36) Konstantakou, M.; Stergiopoulos, T. A Critical Review on Tin Halide Perovskite Solar Cells. *J. Mater. Chem. A* **2017**, *5*, 11518−11549.
(37) Polman, A.; Knight, M.; Garnett, E. C.; Ehrler, B.; Sinke, W. C. Photovoltaic Materials: Present Efficiencies and Future Challenges. *Science* **2016**, *352*, aad4424.
(38) Hao, F.; Stoumpos, C. C.; Cao, D. H.; Chang, R. P. H.; Kanatzidis, M. G. Lead-Free Solid-State Organic−Inorganic Halide Perovskite Solar Cells. *Nat. Photonics* **2014**, *8*, 489−494.
(39) Noel, N. K.; Stranks, S. D.; Abate, A.; Wehrenfennig, C.; Guarnera, S.; Haghighirad, A.-A.; Sadhanala, A.; Eperon, G. E.; Pathak, S. K.; Johnston, M. B.; Petrozza, A.; Herz, L. M.; Snaith, H. J. Lead-Free Organic−Inorganic Tin Halide Perovskites for Photovoltaic Applications. *Energy Environ. Sci.* **2014**, *7*, 3061−3068.
(40) Ke, W.; Stoumpos, C. C.; Spanopoulos, I.; Mao, L.; Chen, M.; Wasielewski, M. R.; Kanatzidis, M. G. Efficient Lead-Free Solar Cells Based on Hollow {en}$MASnI_3$ Perovskites. *J. Am. Chem. Soc.* **2017**, *139*, 14800−14806.
(41) Ke, W.; Stoumpos, C. C.; Zhu, M.; Mao, L.; Spanopoulos, I.; Liu, J.; Kontsevoi, O. Y.; Chen, M.; Sarma, D.; Zhang, Y.; Wasielewski, M. R.; Kanatzidis, M. G. Enhanced PV Performance and Stability with a New Type of Hollow 3D Perovskite {en}$FASnI_3$. *Sci. Adv.* **2017**, *3*, No. e1701293.
(42) Ke, W.; Stoumpos, C. C.; Spanopoulos, I.; Chen, M.; Wasielewski, M. R.; Kanatzidis, M. G. Diammonium Cations in the $FASnI_3$ Perovskite Structure Lead to Lower Dark Currents and More Efficient Solar Cells. *ACS Energy Lett.* **2018**, *3*, 1470−1476.
(43) Song, T.-B.; Yokoyama, T.; Logsdon, J.; Wasielewski, M. R.; Aramaki, S.; Kanatzidis, M. G. Piperazine Suppresses Self-Doping in $CsSnI_3$ Perovskite Solar Cells. *ACS Appl. Energy Mater.* **2018**, *1*, 4221−4226.
(44) Song, T.-B.; Yokoyama, T.; Stoumpos, C. C.; Logsdon, J.; Cao, D. H.; Wasielewski, M. R.; Aramaki, S.; Kanatzidis, M. G. Importance of Reducing Vapor Atmosphere in the Fabrication of Tin-Based Perovskite Solar Cells. *J. Am. Chem. Soc.* **2017**, *139*, 836−842.
(45) Song, T.-B.; Yokoyama, T.; Aramaki, S.; Kanatzidis, M. G. Performance Enhancement of Lead-Free Tin-Based Perovskite Solar Cells with Reducing Atmosphere-Assisted Dispersible Additive. *ACS Energy Lett.* **2017**, *2*, 897−903.
(46) Liu, M.; Johnston, M. B.; Snaith, H. J. Efficient Planar Heterojunction Perovskite Solar Cells by Vapour Deposition. *Nature* **2013**, *501*, 395−398.
(47) Jung, M.-C.; Raga, S. R.; Qi, Y. Properties and Solar Cell Applications of Pb-Free Perovskite Films Formed by Vapor Deposition. *RSC Adv.* **2016**, *6*, 2819−2825.
(48) Wang, N.; Zhou, Y.; Ju, M.-G.; Garces, H. F.; Ding, T.; Pang, S.; Zeng, X. C.; Padture, N. P.; Sun, X. W. Heterojunction-Depleted Lead-Free Perovskite Solar Cells with Coarse-Grained B-γ-$CsSnI_3$ Films. *Adv. Energy Mater.* **2016**, *6*, 1601130.
(49) Ke, W.; Priyanka, P.; Vegiraju, S.; Stoumpos, C. C.; Spanopoulos, I.; Soe, C. M. M.; Marks, T. J.; Chen, M.-C.; Kanatzidis, M. G. Dopant-Free Tetrakis-Triphenylamine Hole Transporting Material for Efficient Tin-Based Perovskite Solar Cells. *J. Am. Chem. Soc.* **2018**, *140*, 388−393.
(50) Zhao, Z.; Gu, F.; Li, Y.; Sun, W.; Ye, S.; Rao, H.; Liu, Z.; Bian, Z.; Huang, C. Mixed-Organic-Cation Tin Iodide for Lead-Free Perovskite Solar Cells with an Efficiency of 8.12%. *Adv. Sci.* **2017**, *4*, 1700204.
(51) Liu, J.; Ozaki, M.; Yakumaru, S.; Handa, T.; Nishikubo, R.; Kanemitsu, Y.; Saeki, A.; Murata, Y.; Murdey, R.; Wakamiya, A. Lead-Free Solar Cells Based on Tin Halide Perovskite Films with High Coverage and Improved Aggregation. *Angew. Chem., Int. Ed.* **2018**, *57*, 13221−13225.
(52) Li, Z.; Klein, T. R.; Kim, D. H.; Yang, M.; Berry, J. J.; van Hest, M. F. A. M.; Zhu, K. Scalable Fabrication of Perovskite Solar Cells. *Nat. Rev. Mater.* **2018**, *3*, 18017.
(53) Lee, S. J.; Shin, S. S.; Kim, Y. C.; Kim, D.; Ahn, T. K.; Noh, J. H.; Seo, J.; Seok, S. I. Fabrication of Efficient Formamidinium Tin Iodide Perovskite Solar Cells through SnF_2-Pyrazine Complex. *J. Am. Chem. Soc.* **2016**, *138*, 3974−3977.
(54) Ding, B.; Li, Y.; Huang, S.-Y.; Chu, Q.-Q.; Li, C.-X.; Li, C.-J.; Yang, G.-J. Material Nucleation/Growth Competition Tuning towards Highly Reproducible Planar Perovskite Solar Cells with Efficiency Exceeding 20%. *J. Mater. Chem. A* **2017**, *5*, 6840−6848.

DOI: 10.1021/acsami.8b19143
ACS Appl. Mater. Interfaces 2019, 11, 3053−3060

(55) Li, Y.; He, X.-L.; Ding, B.; Gao, L.-L.; Yang, G.-J.; Li, C.-X.; Li, C.-J. Realizing Full Coverage of Perovskite Film on Substrate Surface during Solution Processing: Characterization and Elimination of Uncovered Surface. *J. Power Sources* **2016**, *320*, 204−211.
(56) Kayesh, M. E.; Chowdhury, T. H.; Matsuishi, K.; Kaneko, R.; Kazaoui, S.; Lee, J.-J.; Noda, T.; Islam, A. Enhanced Photovoltaic Performance of $FASnI_3$-Based Perovskite Solar Cells with Hydrazinium Chloride Coadditive. *ACS Energy Lett.* **2018**, *3*, 1584−1589.
(57) Lin, K.-F.; Chang, S. H.; Wang, K.-H.; Cheng, H.-M.; Chiu, K. Y.; Lee, K.-M.; Chen, S.-H.; Wu, C.-G. Unraveling the High Performance of Tri-iodide Perovskite Absorber Based Photovoltaics with a Non-Polar Solvent Washing Treatment. *Sol. Energy Mater. Sol. Cells* **2015**, *141*, 309−314.
(58) Gao, L.-L.; Liang, L.-S.; Song, X.-X.; Ding, B.; Yang, G.-J.; Fan, B.; Li, C.-X.; Li, C.-J. Preparation of Flexible Perovskite Solar Cells by a Gas Pump Drying Method on a Plastic Substrate. *J. Mater. Chem. A* **2016**, *4*, 3704−3710.
(59) Ke, W.; Stoumpos, C. C.; Logsdon, J. L.; Wasielewski, M. R.; Yan, Y.; Fang, G.; Kanatzidis, M. G. TiO_2−ZnS Cascade Electron Transport Layer for Efficient Formamidinium Tin Iodide Perovskite Solar Cells. *J. Am. Chem. Soc.* **2016**, *138*, 14998−15003.
(60) Ryu, S.; Noh, J. H.; Jeon, N. J.; Kim, Y. C.; Yang, W. S.; Seo, J.; Seok, S. I. Voltage Output of Efficient Perovskite Solar Cells with High Open-Circuit Voltage and Fill Factor. *Energy Environ. Sci.* **2014**, *7*, 2614−2618.

DOI: 10.1021/acsami.8b19143
ACS Appl. Mater. Interfaces 2019, 11, 3053−3060